

## Angular momentum transfer in the deep inelastic reactions of 237 MeV $^{40}\text{Ar}$ with $^{89}\text{Y}$

M. N. Namboodiri, J. B. Natowitz, P. Kasiraj, R. Eggers,\* L. Adler, P. Gonthier, C. Cerruti,<sup>†</sup> and S. Simon  
*Cyclotron Institute, Texas A & M University, College Station, Texas 77843*

(Received 3 April 1979)

The mechanisms of strongly damped collisions of 237 MeV  $^{40}\text{Ar}$  with  $^{89}\text{Y}$  have been studied by measurements of the energy distributions and angular distributions of the identified products. Average gamma-ray multiplicities  $\langle M_\gamma \rangle$  and average gamma-ray energies  $\langle E_\gamma \rangle$  have been measured for these reactions. Empirical relationships between  $\langle M_\gamma \rangle$  and the average angular momenta were employed to determine the angular momenta of the primary fragments produced in the reactions. The angular momentum transfer in the strongly damped collisions increases with increasing angle of emission of the projectile-like fragment. Evidence is presented that for the lowest partial waves contributing to strongly damped collisions the condition of rigid rotation is achieved. The use of such reactions to select nuclei of particular  $\langle J \rangle$  is discussed.

NUCLEAR REACTIONS  $^{89}\text{Y}$ , ( $^{40}\text{Ar}$ , X),  $E=237$  MeV, deep inelastic collisions; Measured angular distributions, energy spectra and average gamma-ray multiplicities, deduced primary fragment angular momenta.

### I. INTRODUCTION

The determination of angular momentum transfers in deep inelastic reactions can provide detailed information on the reaction mechanism and on the range of partial waves contributing to the reactions.<sup>1-4</sup> In this work we have used measurements of the average total multiplicities  $\langle M_\gamma \rangle$  and average energies  $\langle E_\gamma \rangle$  of continuum  $\gamma$  rays to extract the average  $\gamma$ -ray multiplicities  $\langle M_\gamma \rangle_H$  of the heavier partners of the deep inelastic and fission reactions of  $^{40}\text{Ar} + ^{89}\text{Y}$  at 237 MeV. We then employ data on  $\langle M_\gamma \rangle$  from fusion reactions to derive the angular momenta of the primary heavy fragments produced in the fission and fissionlike processes.

Our results indicate that angular momentum transfer is a slower process than energy damping, but that the composite dinuclear system does achieve the condition of rigid rotation for initial partial waves just above those leading to fusion.

### II. EXPERIMENTAL PROCEDURE

A detector telescope employing a gas ionization  $\Delta E$  detector and an Si  $E$  detector<sup>5</sup> was used to detect and identify products of the collisions of 237 MeV  $^{40}\text{Ar}$  with  $^{89}\text{Y}$ . Angular distributions and energy distributions of products with atomic numbers from 9 to 30 were obtained. Reliable data for the distributions of lighter products were not obtained because of problems of target contamination.

In a separate experiment three  $7.6 \times 7.6$  cm NaI detectors placed at  $35^\circ$ ,  $90^\circ$ , and  $135^\circ$  relative to the incident beam direction were employed to detect the continuum  $\gamma$  rays in coincidence with

identified reaction products detected at laboratory angles ranging from  $25^\circ$  to  $55^\circ$ . The measurements were normally made with the heavy ion telescope in the same plane as the NaI detectors but on the opposite side of the beam. One measurement was made with the heavy ion telescope at  $55^\circ$  in the plane perpendicular to that containing the NaI detectors.

Measured response functions of the NaI crystals were used in the analysis of the pulse height spectra to extract  $\langle M_\gamma \rangle$  the average  $\gamma$ -ray multiplicity of the reaction, and  $\langle E_\gamma \rangle$  the average  $\gamma$ -ray energy. Both the experimental and analytical techniques are described in detail in Ref. 6.

### III. RESULTS

#### A. Energy and angular distributions

Observations of strongly damped collisions of  $^{40}\text{Ar}$  projectiles with several different target nuclei have previously been reported.<sup>7-9</sup> The same characteristic reaction features reported in those studies are observed in the present work. In particular, the data show an increasing relaxation of the product energy spectra with increasing difference between the projectile mass and the mass of the observed product, or with increasing angle beyond the grazing angle. This is obvious from Fig. 1 where the most probable energies of  $Z$ -identified products are plotted for different angles of observation. The conversion of the measured laboratory energies to the center-of-mass system utilizes the mass of the detected product. We have assumed that for each  $Z$ , the mass is that of the isotope closest to the line of  $\beta$  stability. Using the most probable fragment energies, we have converted the laboratory angular distributions

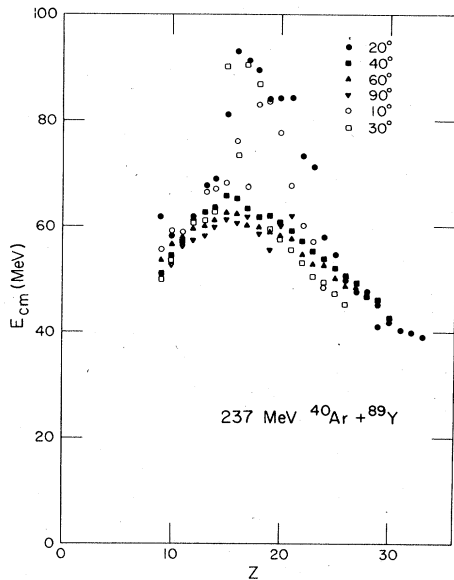


FIG. 1. Most probable center-of-mass kinetic energy for  $Z$  identified products. The energies are plotted against  $Z$  for six different laboratory angles. These energies are uncertain by  $\pm 5\%$ .

to the center of mass.

The resultant angular distributions  $(d\sigma/d\theta)_{c.m.}$  are depicted in Fig. 2. Angular distributions of products with atomic numbers near the projectile atomic number are forward peaked, but show a decreasing angular dependence as the difference between the projectile and product atomic numbers increases. For the heaviest products with  $Z \geq 23$  it appears that the high angular momentum limit of a constant  $d\sigma/d\theta$  is reached.

The elemental yield distributions of the strongly damped products are more easily viewed in Fig. 3 where  $(d\sigma/d\theta)_{c.m.}$  is plotted against product atomic number at two different center-of-mass angles. The values plotted were obtained from smooth lines drawn through the data presented in Fig. 2. The presence of two different components in the elemental yield distribution is clearly suggested by the data: a lower  $Z$  component for which both the centroid and magnitude change with increasing center-of-mass angle and a higher  $Z$  component for which the centroid and magnitude are independent of the center-of-mass angle. The shaded region on the plot indicates the apparent yield distribution of this latter component, assuming it is symmetric.

The lower  $Z$  component exhibits the characteristics of strongly damped reaction processes in which the width of the  $Z$  distribution of the projectile-like fragments increases and the position of the centroid of that distribution shifts toward symmetry as the interaction time (scattering

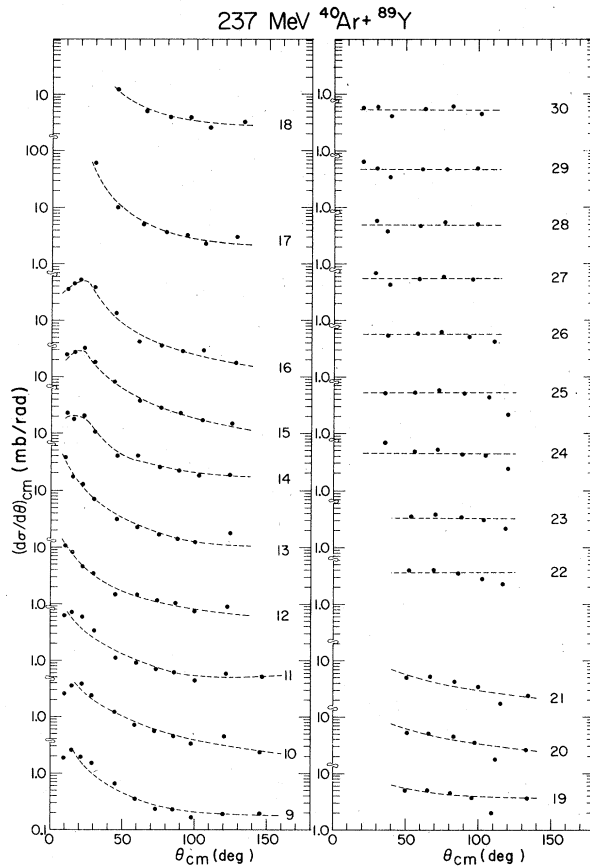


FIG. 2. Center-of-mass differential cross sections  $d\sigma/d\theta$ . The laboratory data have been transformed using the most probable energy of the observed distributions.

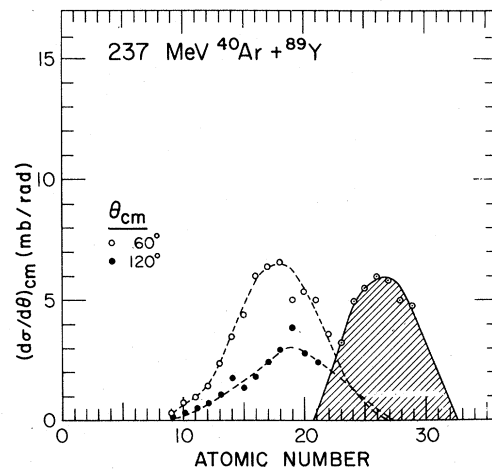


FIG. 3. Center-of-mass elemental yield distributions. Data are presented for  $60^\circ$  and  $120^\circ$ . The yield of the lower  $Z$  component decreases with angle. The yield of the higher  $Z$  component remains constant.

angle) increases.<sup>10,11</sup>

For the higher  $Z$  component on the other hand, the constancy of the magnitude and position of the yield distribution indicates that the scissioning system has a lifetime long compared to the rotational time of the composite nucleus. This higher component results either from strongly damped collisions in which orbiting occurs or from fusion-fission. The magnitude of the yield suggests that fusion-fission may be an important contributor to this component.

### B. Gamma-ray multiplicities

The results of our  $\gamma$ -ray multiplicity measurements are presented in Fig. 4. For detected

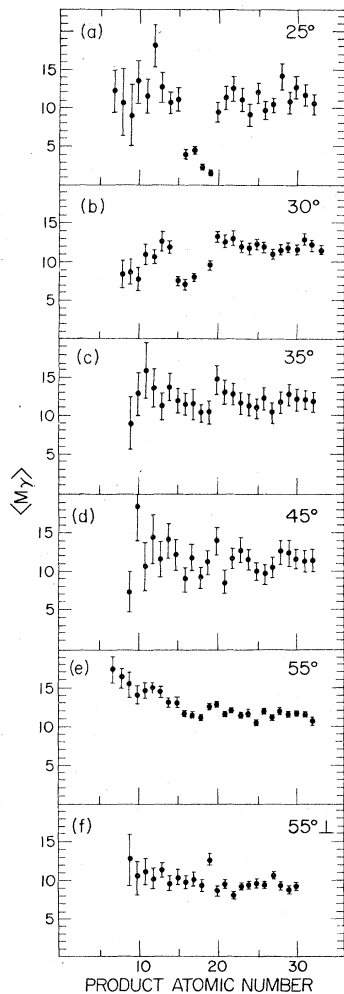


FIG. 4. Average  $\gamma$ -ray multiplicities  $\langle M_\gamma \rangle$  as a function of the atomic number of the coincident identified product. Data were taken with the heavy ion telescope at five different laboratory angles. In parts (a)–(e) the NaI detectors were in the same plane as the heavy ion telescope. The data in (f) were taken with an NaI detector placed perpendicular to the plane containing the heavy ion telescope.

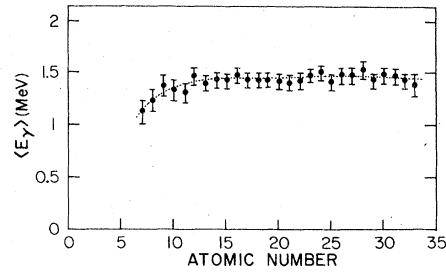


FIG. 5. Average  $\gamma$ -ray energy  $\langle E_\gamma \rangle$  as a function of the atomic number of the identified coincident product. Data were taken with the heavy ion telescope at  $55^\circ$  as in part (e) of Fig. 4.

fragments with the highest atomic numbers, the measured reaction  $\gamma$ -ray multiplicities are in the neighborhood of 11.5 for all measurements in which the  $\gamma$ -ray detectors were positioned in the reaction plane defined by the heavy ion telescope. For detected fragments with intermediate atomic numbers near that of the projectile, very low reaction multiplicities are observed at angles where the energy spectra show little relaxation, while at larger fragment angles the multiplicity increases significantly. A large increase in reaction multiplicity with fragment detection angle also occurs when products of lower atomic number are detected, although in these cases the energy spectra are strongly damped at all angles of observation.

In Fig. 5 the average  $\gamma$ -ray energies  $\langle E_\gamma \rangle$  observed for the spectra corresponding to fragment detection at  $55^\circ$  are presented. These data are useful in understanding the relative contributions of heavy and light fragment deexcitation to  $\langle M_\gamma \rangle$  as is discussed in the following section.

## IV. DISCUSSION

### A. Reaction mechanism

Earlier reaction studies using  $A = 40$  projectiles in the 5 to 10 MeV/nucleon energy range have demonstrated that both fusion and deep inelastic processes account for significant fractions of the total reaction probability.<sup>7-9, 12-16</sup> Some previously reported evaporation residue cross sections and fission cross sections are shown in Fig. 6. Interpolation of the evaporation residue cross section measurements for projectiles with energies near 230 MeV suggests that the evaporation residue cross section in the system studied here should be  $\sim 750$  mb.

Integration of the yields of the high  $Z$  symmetric component in the distributions presented in Fig. 3 results in a differential cross section  $(d\sigma/d\theta)_{c.m.}$  of  $42.3 \pm 5$  mb/radian. For a constant  $(d\sigma/d\theta)_{c.m.}$ , one half of the angle integrated cross section is  $66.4 \pm 8$  mb. This cross section which constitutes

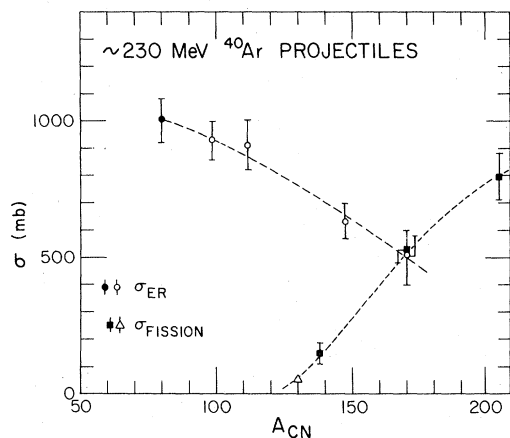


FIG. 6. Experimental evaporation residue and fission cross sections for  $A = 40$  projectiles. Data obtained for projectile energies near 230 MeV and reported in Refs. 12-16 are shown. The point at  $A_{cn} = 80$  results from experiments using  $^{40}\text{Ca}$ , the others from experiments with  $^{40}\text{Ar}$ .

at least an upper limit to the fusion-fission cross section is in good agreement with the trend of the previously reported fission cross sections as shown in Fig. 6. Adding this cross section to the interpolated evaporation residue cross section leads to an estimated fusion cross section of  $810 \pm 100$  mb. Applying the sharp cutoff approximation suggests a limiting angular momentum for fusion of  $(75 \pm 5)\hbar$ . The grazing angular momentum for this system is expected to be  $116\hbar$ .

There are then many partial waves available for which strong interactions not leading to compound nucleus formation can occur. Various models have been proposed to describe such strongly damped collision processes.<sup>10,17-20</sup> Models based on macroscopic approaches employing the concepts of friction and diffusion have provided some significant insights into the reaction mechanism. The link between the macroscopic features and microscopic behavior is still being explored.<sup>21</sup> One of us (C.C.) has developed a code based upon the friction model approach but including particle transfer and its effect on the projectile trajectory during the damping process. This code has been very successful in describing the cross sections and mass distributions for deep inelastic reactions of lighter systems.<sup>20</sup>

Applied to this system, the calculation of Cerruti predicts a limiting angular momentum for fusion of  $66\hbar$  in reasonable agreement with the estimate based upon our interpolation of evaporation residue cross section measurements. For higher partial waves fusion does not occur, but partial waves near the fusion limit undergo large angular deflections corresponding to long interaction times in which large changes in the mass

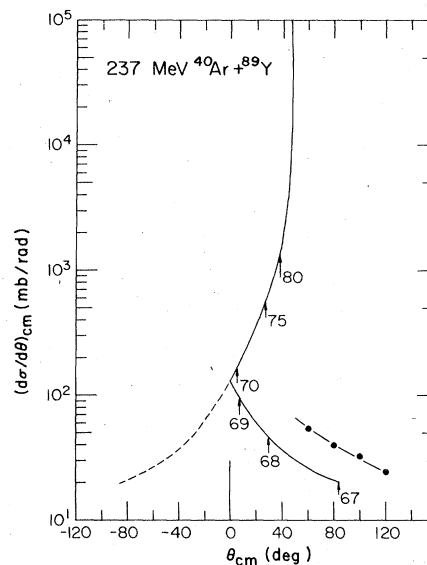


FIG. 7. Calculated mean angular distribution for projectile-like fragments. The arrows indicate the center-of-mass angle associated with particular incident partial waves. The solid points show the experimental cross sections determined for the lower  $Z$  component of the yield distribution of strongly damped collisions as observed in Fig. 3.

distribution, the kinetic energy, and the orbital angular momentum are predicted.

In particular, the calculated mean center of mass angular distribution of the projectile-like fragments is shown in Fig. 7. For the partial waves just above the fusion limit the calculation leads to trajectories which orbit through  $0^\circ$ . The scattering angle and differential cross section calculated for some particular partial waves are indicated by arrows in the figure. Neglecting fluctuations, products observed at large scattering angles are predicted to result from partial waves near 67-68 immediately above the calculated fusion limit.

For comparison with these predictions, cross sections obtained by integration of the yields of elements in the lower  $Z$  component in the distributions of fissionlike products are also shown. The resultant cross sections  $(d\sigma/d\theta)_{c.m.}$  at four different c.m. angles, presented in Fig. 7, are found to be approximately twice as large as those calculated, but to decrease at essentially the same rate with  $\theta_{c.m.}$ . This result suggests that the calculation provides a good approximation to the experimental mean deflection function but that the actual interaction times may be slightly longer than those calculated.

#### B. Angular momentum transfer

A particular goal of the present experiments was to employ multiplicity measurements to study

angular momentum transfer in the strongly damped collisions. In order to obtain information on the angular momenta of the products of strongly damped collisions, it is first necessary that individual product multiplicities be deduced from the measured reaction multiplicities. Following that, the conversion of multiplicity to angular momentum can be made if the relationship between the two is known.

Some data relating  $\gamma$ -ray multiplicity and angular momenta are presented in Fig. 8.<sup>6,22-27</sup> This figure is a contour diagram of the results of recent measurements of  $\langle M_\gamma \rangle$  for a number of fusion reactions. The data are plotted as a function of the mass and the average angular momentum of the deexciting compound nucleus. The values of  $\langle J \rangle$  have been determined by applying the sharp cutoff model to measured fusion cross section data where such data are available. In the absence of the appropriate cross section data, the values have been determined from a Bass model calculation of the limiting angular momentum for fusion. This figure differs only slightly from that presented in Ref. 28.

It is clear from the figure that the  $\gamma$ -ray multiplicities are relatively sensitive to angular momentum for  $A \geq 70$  and relatively insensitive to angular momentum at lower masses. Presumably this insensitivity at lower masses reflects the importance of the particle emission cascade as a means of angular momentum dissipation.

The excitation energies of the compound nuclei for which data are presented in Fig. 8 vary con-

siderably. Since the multiplicity for a particular  $\langle J \rangle$  can also depend somewhat on the excitation energy, it would clearly be advantageous to have additional data to construct a more refined  $\langle M_\gamma \rangle$  versus  $\langle J \rangle$  calibration plot. Insufficient data are now available. However, in view of the fact that thermal equilibrium appears to be a very good assumption in completely damped collisions,<sup>29</sup> the excitation energies of the heavier reaction products studied here should in fact be quite comparable to those for which the multiplicity data presented in Fig. 8 were taken.

Thus, the dependence of  $\langle M_\gamma \rangle$  on  $A_{CN}$  and  $\langle J \rangle$  as expressed in the contours of Fig. 8 is the basis of our translation of product  $\gamma$ -ray multiplicities to product angular momenta. Inherent in this approach is the additional assumption that the multiplicity reflects the average angular momentum and that differences between the angular momentum distributions of the compound nuclei produced in fusion reactions and those of the nuclei produced in deep inelastic reactions do not significantly alter these  $\gamma$ -ray multiplicities.

It should be emphasized that even though the average angular momenta are determined from measurements of  $\langle M_\gamma \rangle$ , the effects of particle emission or fission on the observed multiplicities are automatically taken into account by the calibration technique.

The utilization of the information in Fig. 8 clearly requires that the individual product multiplicities be known. For the system studied here, two methods of separating the measured reaction multiplicities into individual product multiplicities may be employed. In the first, it is simply necessary to recognize that for nuclei with mass less than  $\sim 50$  the  $\gamma$ -ray multiplicity is essentially independent of angular momentum. Therefore in asymmetric breakups in which one of the final partners has a mass number less than 50, the contribution to the reaction multiplicity from that partner can be determined with relatively small uncertainties. For symmetric breakups the average multiplicities of the two partners should be identical. Since symmetric breakup for the system studied here leads to mass numbers in the range of 65, for products in the mass number range 50–65 a reasonable multiplicity estimate could be made by interpolation observed for mass 50 and mass 65 products assuming a smooth variation with mass.

In the second method a quantitative decomposition of the reaction multiplicities  $\langle M_\gamma \rangle_H$  and  $\langle M_\gamma \rangle_L$  associated with the heavy and light fragments is made possible by the fact that the average  $\gamma$ -ray energies of the products of interest in this investigation are a function of the mass number. This is

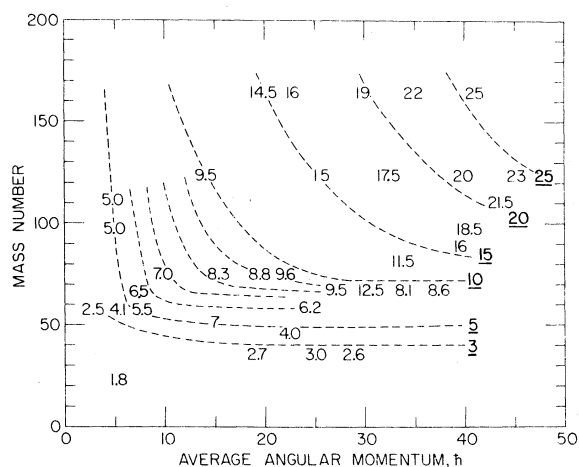


FIG. 8. Average  $\gamma$ -ray multiplicities as a function of mass and average angular momentum. The measured multiplicities reported for compound nucleus deexcitation (Refs. 6, 22–27) are presented. The dashed lines indicate the assumed contours of constant multiplicity which have been utilized in this work.

illustrated in Fig. 9 where various data on the average energies  $\langle E_\gamma \rangle$  are presented as a function of the mass of the  $\gamma$ -decaying nucleus.<sup>6, 22-27, 30</sup>

We assume once again that the mass of the detected fragment corresponds to the line of  $\beta$  stability and therefore that both masses may be determined from the measured atomic number with sufficient accuracy to determine the average energies  $\langle E_\gamma \rangle_H$  and  $\langle E_\gamma \rangle_L$  from Fig. 9. We then use the relationships

$$\langle M_\gamma \rangle_H \langle E_\gamma \rangle_H + \langle M_\gamma \rangle_L \langle E_\gamma \rangle_L = \langle M_\gamma \rangle \langle E_\gamma \rangle, \quad (1)$$

$$\langle M_\gamma \rangle_H + \langle M_\gamma \rangle_L = \langle M_\gamma \rangle \quad (2)$$

to extract the multiplicities  $\langle M_\gamma \rangle_H$  and  $\langle M_\gamma \rangle_L$  from the measured reaction multiplicity  $\langle M_\gamma \rangle$ .

In Fig. 5 the average  $\gamma$ -ray energies of the  $\gamma$  spectra observed in coincidence with fragments detected in the telescope at  $55^\circ$  to the beam direction were presented. The data are the same as those from which the values of  $\langle M_\gamma \rangle$  were obtained. We have represented the  $\langle M_\gamma \rangle$  and  $\langle E_\gamma \rangle$  data by smooth functions through the experimental points and then decomposed the multiplicity according to Eqs. (1) and (2). The results of such an analysis are presented in Fig. 10. The solid circles in that figure represent the multiplicities  $\langle M_\gamma \rangle_H$  of the heavier reaction partner. For large mass asymmetries, the major fraction of the  $\gamma$  rays clearly result from the heavier products. The lighter partners have low multiplicities  $\sim 2$  to  $3$  over a wide mass range. As mass symmetry is approached, the sudden decrease in  $\langle M_\gamma \rangle_H$  and the increase in  $\langle M_\gamma \rangle_L$  occur near entrance into a mass region where the multiplicity becomes more sensitive to mass changes and less sensitive to angular momentum changes.

Note that the values of  $\langle M_\gamma \rangle_L$  which are derived by this method are in fact consistent with the expectations based on Fig. 8. In the region of product

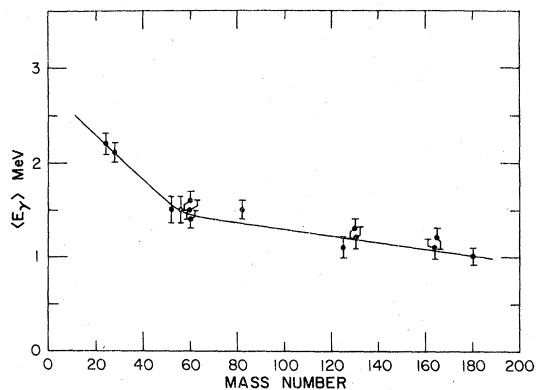


FIG. 9. Average  $\gamma$ -ray energies as a function of mass. Data are from Refs. 6, 22-27, 30.

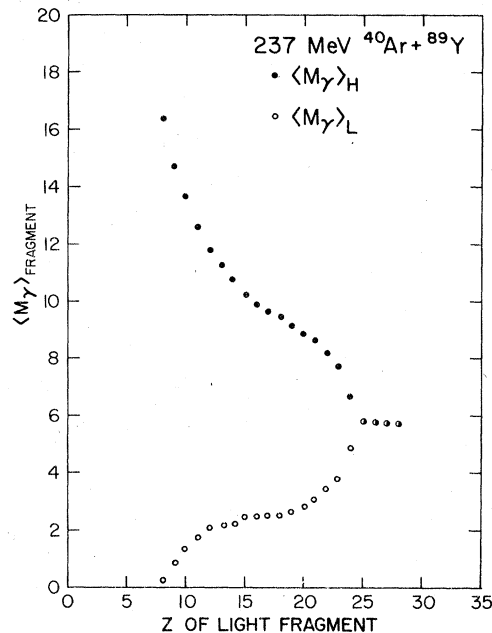


FIG. 10. Decomposition of the reaction multiplicity  $\langle M_\gamma \rangle$ . The method described in the text has been applied to the smoothed average  $\gamma$ -ray multiplicities to extract the multiplicities  $\langle M_\gamma \rangle_L$  and  $\langle M_\gamma \rangle_H$  of the two fragments produced in the deep inelastic reactions. Data are those of Fig. 4(e).

atomic number 10-20 (mass range  $\sim 20$ -40) the multiplicities  $\langle M_\gamma \rangle_L$  are close to 2.5, and the reaction multiplicities are dominated by  $\langle M_\gamma \rangle_H$ . As the mass split becomes more symmetric the values of  $\langle M_\gamma \rangle_L$  and  $\langle M_\gamma \rangle_H$  converge. It is certainly expected that for very large angular momenta there can be significant changes in  $\langle E_\gamma \rangle$ . The observed trends<sup>31, 32</sup> for compound systems in the mass region near  $A = 100$  indicate that such shifts are not important in the range of fragment angular momenta encountered here. This interpretation is further supported by the consistency between the analysis employing  $\langle E_\gamma \rangle$  and the trends indicated in Fig. 8.

Using the derived values of  $\langle M_\gamma \rangle_H$  and the calibration data presented in Fig. 8, we have determined the angular momenta of the heavy primary fragments. These angular momenta are plotted in Fig. 11.

The large increase of fragment angular momentum with increasing asymmetry of the scissioning composite nucleus indicates that the system approaches a sticking condition. In the limit, such a condition is expected to lead to a rigid rotation of the composite system in which the initial orbital angular momentum is partitioned according to the moments of inertia of the fragments and of the composite system.<sup>33</sup>

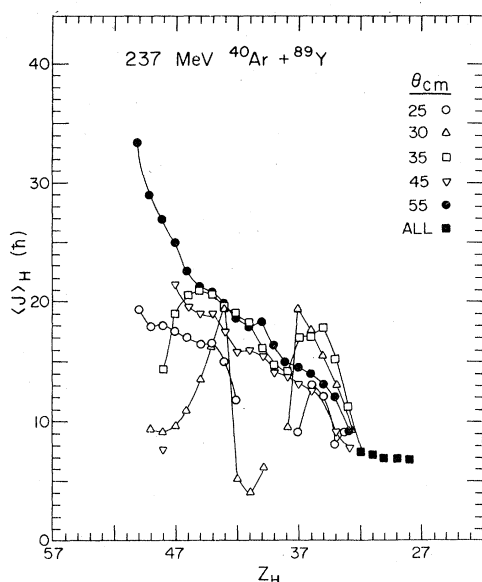


FIG. 11. Average angular momenta  $\langle J \rangle_H$  as a function of atomic number. Data are presented for five different laboratory angles. Error bars are omitted for clarity but the relative errors should be comparable to those presented in Fig. 4.

Is rigid rotation in fact achieved in this system? To answer this question we note that the information on fragment kinetic energies presented in Fig. 1 can be employed to provide information on the scission shape and therefore on the relative moments of inertia of the composite nucleus.

We assume a shape parametrization of the scissioning system consisting of two ellipsoids in contact along the direction of their major axes. For a rigidly rotating system, the observed total kinetic energy of the fragments should be a combination of the Coulomb and rotational energies

$$E_K = \frac{z_1 z_2 e^2}{d} + f \frac{\hbar^2 l(l+1)}{2\mu d^2}, \quad (3)$$

where  $l$  is the initial orbital angular momentum,  $d$  is the separation distance of the fragment centers at scission, and  $f$  (also a function of  $d$ ), is the ratio  $I_0/(I_0 + I_1 + I_2)$  where  $I_0$  is the moment of inertia of the composite system and  $I_1$  and  $I_2$  are the fragment moments of inertia. We note that  $E_K$  depends upon both  $l$  and  $d$ .

Application of momentum conservation to the evaporation-corrected fragment kinetic energy data presented in Fig. 1 allows us to determine the experimental total kinetic energies as a function of mass asymmetry. For different assumed values of  $l$  and experimental kinetic energies  $E_K$ , Eq. (3) may be used to determine both  $d$  and  $f$ . The derived values of  $d$ , using the model, indicate that

the ratio of semimajor to semiminor axes of the heavier fragment ranges from 1.5 at symmetry to 1.3 for the most asymmetric splits reported. Since the intrinsic angular momentum of the fragments is  $(1-f)l$  and is split between them according to the individual moments of inertia, it is possible to calculate  $\langle J \rangle_H$  for each assumed value of  $l$ .

In Fig. 12 the results of such calculations for  $l=40$ , 70, and 100 are presented as dashed lines. The experimentally determined values of  $\langle J \rangle_H$  corresponding to detection of the projectile-like fragments at  $55^\circ$  in the laboratory are also plotted. The error bars represent only errors on the multiplicity determination. No uncertainty in the multiplicity to angular momentum conversion is included.

Over the entire product mass range, the variation of  $\langle J \rangle_H$  with mass asymmetry and the magnitudes of  $\langle J \rangle_H$  are in very good agreement with the values calculated for rigid rotation of a composite system formed in collisions with projectile partial waves near 70.

Since the products corresponding to near symmetric mass splits may result from fission of the compound nucleus, the results indicate that such fission would occur predominantly from the com-

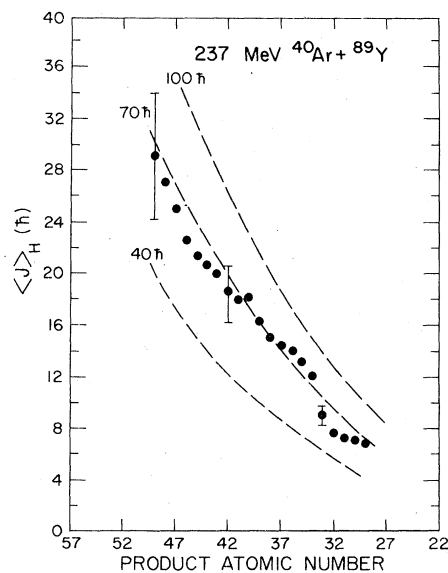


FIG. 12. Comparison between experimental and calculated values of  $\langle J \rangle_H$ . Data from observation of the projectile-like fragment at  $55^\circ$  are indicated by solid circles. Calculated values for three different assumed initial angular momenta were obtained by utilizing the fragment kinetic energy to provide information on the nuclear deformation and assuming rigid rotation of the deformed system. The value of  $70\hbar$  is very close to the limiting angular momentum for evaporation residue production.

pound nuclei with the highest angular momenta. For the other nuclei which result from strongly damped collisions, the results indicate that the products observed at  $55^\circ$  are indeed produced in collisions with projectiles having orbital angular momenta near the sharp cutoff fusion limit and further that rigid rotation is in fact achieved.

The decrease in apparent multiplicity when the  $\gamma$  rays are observed perpendicular to the reaction plane indicates an alignment of the  $\gamma$ -emitting nuclei. The magnitude of this alignment is difficult to determine without detailed information on the nature of the  $\gamma$ -ray cascade. The recent determinations of the multiplicity and multipolarity<sup>31,32</sup> of  $\gamma$  rays emitted in the deexcitation of the compound nucleus  $^{122}\text{Te}$  lead to the conclusion that the  $\gamma$  cascade is approximately 60% stretched quadrupole and 40% stretched dipole for nuclei having angular momenta such as those indicated for the heaviest fragments we have investigated. For 100% alignment perpendicular to the reaction plane, such a cascade would lead to an in-plane to out-of-plane anisotropy,  $\omega(90^\circ)/\omega(0^\circ) = 1.8$ . The measured anisotropy associated with fragments detected at  $55^\circ$  is 1.3, indicating that there is in fact a strong fragment alignment even after particle emission.

Glässel *et al.*<sup>2</sup> have previously reported values  $\langle M_\gamma \rangle$  for the reactions of 175 MeV  $^{20}\text{Ne}$  and Ag. Since nearly the same composite system is formed in that system as in the system which we have studied, it is possible to apply a very similar analysis.

The reaction multiplicities reported for detection

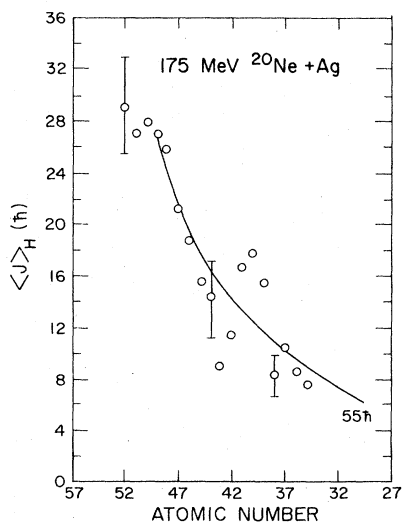


FIG. 13. Comparison between experimental and calculated values of  $\langle J \rangle_H$  for the reaction 175 MeV  $^{20}\text{Ne} + \text{Ag}$ . The analysis utilizes the fragment kinetic energies and the assumption of rigid rotation as described in the text.

of products at  $\theta_L = 90^\circ$  have been separated into  $\langle M_\gamma \rangle_H$  and  $\langle M_\gamma \rangle_L$  by assuming that  $\langle M_\gamma \rangle_L$ , which is very insensitive to angular momentum, follows the same trend with mass asymmetry as that determined for the  $^{40}\text{Ar} + ^{89}\text{Y}$  collisions. From  $\langle M_\gamma \rangle_H$  we have obtained  $\langle J \rangle_H$  from the calibration data in Fig. 8. The results are plotted in Fig. 13.

Babinet *et al.*<sup>34</sup> have reported measurements of the kinetic energies for the products of strongly damped collisions of 175 MeV  $^{20}\text{Ne}$  with Ag. From these values  $E_K$  may be obtained. The expected values of  $\langle J \rangle_H$  can be determined for different assumed values of  $l$ . The line in Fig. 13 represents the results of such a calculation for an initial

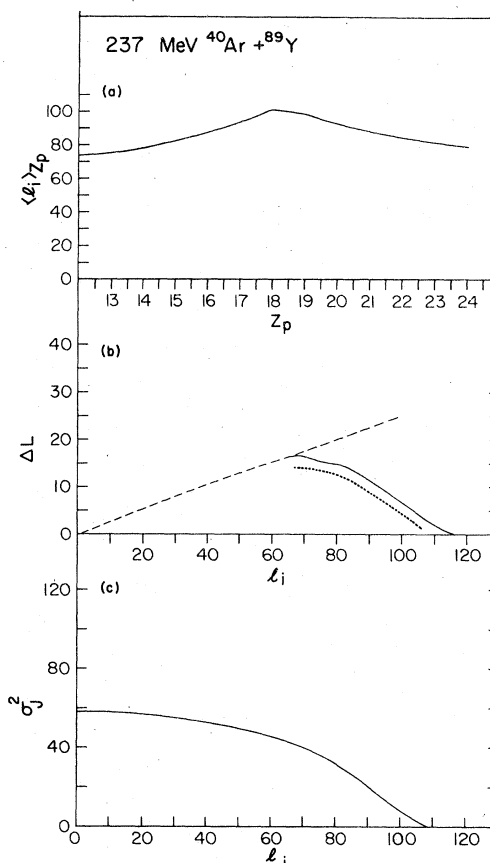


FIG. 14. Calculated properties for strongly damped collisions of 237 MeV  $^{40}\text{Ar}$  with  $^{89}\text{Y}$ . Diffusion model calculations were performed by Wolschin. Part (a) depicts the average initial partial wave leading to projectile-like products of particular atomic number. In part (b) the solid line shows the calculated angular momentum loss  $\Delta L$  as a function of the initial partial wave. The dotted line shows the same property calculated in the model of Cerruti (Ref. 20). Both calculations are for the initial mass asymmetry. The dashed line indicates the limit of rigid rotation. Part (c) presents the calculated variance of the  $Z$  component of the angular momentum distribution as a function of the incident partial wave.

orbital angular momentum of  $55\hbar$ . The experimental limiting angular momentum for fusion in this system has been reported to be  $(57 \pm 7)\hbar$ .<sup>35</sup> Here again, the results indicate that the angle of observation has selected partial waves near the fusion limit and that rigid rotation is reached in such collisions.

Recently Wolschin and Norenberg<sup>36</sup> have proposed a model in which the transfer of angular momentum from collective to intrinsic modes is treated as a diffusion process in the same manner as previous treatments of energy and mass transfer.

The starting point for such a calculation is the variation of interaction time of the projectile and target nuclei with incident partial wave. Such information may be extracted from an experimental mean deflection function of the projectile-like fragment or alternatively may be obtained from a suitable dynamic calculation. Since the calculations of Cerruti are in good general agreement with the basic features of the deep inelastic processes, interaction times determined from the dynamic calculation were employed as input to the diffusion calculation. The results of the calculation are shown in Fig. 14. In part (a) the average partial wave leading to a particular element is plotted versus the product atomic number. In part (b) the change  $\Delta L$  in the initial orbital angular momentum is plotted for each partial wave, while in part (c) the variance of the fragment  $M$  distribution is plotted. For the latter two plots, the calculations have been made for a mass asymmetry which is the same as that of the entrance channel. The prediction of the model that rigid rotation is achieved for partial waves near  $68\hbar$  is consistent with the results of our experiments. The model also predicts variances of the  $Z$  component of the angular momentum distribution of 40 when this condition is achieved. These varia-

nces have not been determined in the present experiment, but information on the variances would certainly be useful since the present data indicate that deep inelastic reactions for systems having appreciable fusion cross sections might be very valuable as a means of preparing excited nuclei with well defined high angular momenta. The study of high spin states of nuclei might be significantly simplified by the use of such reactions.

In this regard, we note also that it is expected that angular momentum fractionation occurs as shown in Fig. 14(a). That is, that the average partial wave leading to a particular product mass will vary. Thus selection of a particular mass fractionation might be considered as a means of selecting partial waves. Indeed earlier analyses<sup>2, 28</sup> of the  $\gamma$ -ray experiments represented in Figs. 12 and 13 were interpreted as providing evidence for rigid rotation and also for angular momentum fractionation. While fractionation can be important, the present analysis using a somewhat improved  $\langle M_z \rangle$  calibration and relying on the fragment kinetic energies to provide information on the scission shape indicates that in fact the fragments observed at large  $\theta_z$  do result from a very narrow range of partial waves. Thus for light systems with orbiting type deflection functions, the selection according to angle is a better tool for choosing partial waves.

#### ACKNOWLEDGMENTS

We appreciate the many helpful discussions with G. Wolschin and C. Ngo regarding this work. We also thank Y. Sakurada and the Operations Crew of the TAMU Cyclotron for the Ar beam. This research was supported by the United States Department of Energy and the Robert A. Welch Foundation.

\*Present address: Cyclotron Corporation, Berkeley, California.

†Present address: Institut de Physique Nucléaire, Lyon, France.

<sup>1</sup>H. Kamitsubo, in Proceedings of the Symposium on Macroscopic Features of Heavy Ion Collisions, Report No. ANL/PHY 76-2, 1976 (unpublished), p. 177.

<sup>2</sup>P. Glässel, R. S. Simon, R. M. Diamond, R. C. Jared, I. Y. Lee, L. G. Moretto, J. O. Newton, R. Schmitt, and F. S. Stephens, *Phys. Rev. Lett.* **38**, 331 (1977).

<sup>3</sup>P. Dyer, R. J. Puigh, R. Vandenbosch, T. D. Thomas, and M. S. Zisman, *Phys. Rev. Lett.* **39**, 392 (1977).

<sup>4</sup>A. Olmi, H. Sann, D. Pelte, Y. Eyal, A. Gobbi, W. Kohl, U. Lynen, G. Rudolf, H. Stelzer, and R. Bock, *Phys. Rev. Lett.* **41**, 688 (1978).

<sup>5</sup>M. M. Fowler and R. C. Jared, *Nucl. Instrum. Methods* **124**, 341 (1975).

<sup>6</sup>K. A. Geoffroy, J. B. Natowitz, R. C. Eggers, and M. N. Namboodiri, *Nucl. Phys.* **A302**, 310 (1978).

<sup>7</sup>A. G. Artukh, G. F. Gridnev, V. L. Nikheev, V. V. Volkov, and J. Wilczynski, *Nucl. Phys.* **A215**, 91 (1973).

<sup>8</sup>J. Galin, L. G. Moretto, R. Babinet, R. Schmitt, R. Jared, and S. G. Thompson, *Nucl. Phys.* **A255**, 472 (1975).

<sup>9</sup>B. Gatty, D. Guerreau, M. Lefort, X. Tarrago, J. Galin, B. Cauvin, J. Girard, and H. Nifenecker, *Nucl. Phys.* **A253**, 511 (1975).

<sup>10</sup>W. Nörenberg, *J. Phys. (Paris)* **37**, C5-141 (1976); *Phys. Lett.* **52B**, 289 (1974).

<sup>11</sup>W. U. Schröder, J. R. Birkelund, J. R. Huizenga,

- K. L. Wolf, and V. E. Viola, *Phys. Rev. C* **16**, 623 (1977).
- <sup>12</sup>H. Gauvin, D. Guerreau, Y. LeBeyec, M. Lefort, F. Plasil, and X. Tarrago, *Phys. Lett.* **58B**, 163 (1975).
- <sup>13</sup>H. C. Britt, B. H. Erkkila, R. H. Stokes, H. H. Gutbrod, F. Plasil, R. L. Ferguson, and M. Blann, *Phys. Rev. C* **13**, 1483 (1976).
- <sup>14</sup>B. Tamain, C. Ngo, J. Peter, and F. Hanappe, *Nucl. Phys.* **A252**, 187 (1975).
- <sup>15</sup>P. Colombani, N. Frascaria, J. C. Jacmart, M. Riou, C. Stephan, H. Doubre, N. Poffe, and J. C. Roynette, *Phys. Lett.* **55B**, 45 (1975).
- <sup>16</sup>H. Doubre, A. Gamp, J. C. Jacmart, N. Poffe, J. C. Roynette, and J. Wilczynski, *Phys. Lett.* **73B**, 135 (1978).
- <sup>17</sup>D. H. E. Gross and H. Kalinowski, *Phys. Lett.* **48B**, 302 (1974); D. H. E. Gross, H. Kalinowski, and J. N. De, *Z. Phys.* **A277**, 385 (1976).
- <sup>18</sup>L. G. Moretto and J. S. Sventek, *Phys. Lett.* **56B**, 26 (1975); **65B**, 326 (1976).
- <sup>19</sup>H. Hofmann and C. Ngo, *Phys. Lett.* **65B**, 97 (1976).
- <sup>20</sup>R. Billery, C. Cerruti, A. Chevarier, N. Chevarier, and A. Demeyer, *Z. Phys.* **A285**, 389 (1978).
- <sup>21</sup>T. Tamura and T. Udagawa, *Phys. Lett.*, **82B**, 349 (1979).
- <sup>22</sup>K. A. Geoffroy, J. B. Natowitz, R. Eggers, P. Kasiraj, and M. N. Namboodiri, *Nucl. Phys.* **A302**, 333 (1978).
- <sup>23</sup>J. H. Degnan, B. L. Cohen, G. R. Rao, K. C. Chan, and L. Shabason, *Phys. Rev. C* **6**, 2255 (1973).
- <sup>24</sup>J. R. Beene, O. Hausser, A. J. Ferguson, H. R. Andrews, M. A. Lone, B. Herskind, and C. Broude (unpublished).
- <sup>25</sup>J. O. Newton, I. Y. Lee, R. S. Simon, M. M. Aleonard, Y. El Masri, F. S. Stephens, and R. M. Diamond, *Phys. Rev. Lett.* **38**, 810 (1977).
- <sup>26</sup>J. J. Simpson, P. O. Tjøm, I. Espe, G. B. Hagemann, B. Herskind, and M. Niemen, *Nucl. Phys.* **A287**, 362 (1977).
- <sup>27</sup>N. T. Porile and G. B. Saha, *Phys. Rev.* **158**, 1027 (1967).
- <sup>28</sup>J. B. Natowitz, M. N. Namboodiri, P. Kasiraj, R. Eggers, L. Adler, P. Gonthier, C. Cerruti, and T. Alleman, *Phys. Rev. Lett.* **40**, 751 (1978).
- <sup>29</sup>K. Van Bibber, R. J. Ledoux, S. G. Steadman, F. Videbaek, G. Young and C. Floum, Report No. ANL/PHY 76-2, 1976 (unpublished), Vol. II, p. 811; B. Cauvin, R. C. Jared, P. Russo, R. P. Schmitt, R. Babinet, and L. G. Moretto, *Nucl. Phys.* **A301**, 511 (1978).
- <sup>30</sup>J. F. Mollenauer, *Phys. Rev.* **127**, 867 (1962).
- <sup>31</sup>M. A. Deleplanque, I. Y. Lee, F. S. Stephens, R. M. Diamond, and M. M. Aleonard, *Phys. Rev. Lett.* **40**, 629 (1978).
- <sup>32</sup>M. A. Deleplanque, Th. Byrski, R. M. Diamond, H. Hüber, F. S. Stephens, B. Herskind, and R. Bauer, *Phys. Rev. Lett.* **41**, 1105 (1978).
- <sup>33</sup>C. F. Tsang, *Phys. Scr.* **10**, 90 (1974).
- <sup>34</sup>R. Babinet, L. G. Moretto, J. Galin, R. Jared, J. Moulton, and S. G. Thompson, *Nucl. Phys.* **A258**, 172 (1976).
- <sup>35</sup>F. Plasil and M. Blann, *Phys. Rev. C* **11**, 508 (1975).
- <sup>36</sup>G. Wolschin and W. Norenberg, *Phys. Rev. Lett.* **41**, 691 (1978).